Letter

Microscopic origin of polarization-entangled Stokes–anti-Stokes photons in diamond

Tiago A. Freitas [1,2,3] Paula Machado [2,3] Lucas Valente [2] Diego Sier [2] Raul Corrêa [2] Riichiro Saito [4] Christophe Galland [5] Marcelo F. Santos [6] Carlos H. Monken [2] and Ado Jorio [1,2]

[1]*Programa de Pós-Graduação em Engenharia Elétrica*

[2]*Departamento de Física, Universidade Federal de Minas Gerais, Belo Horizonte, MG 30123-970, Brazil*

[3]*Instituto D'Or de Pesquisa e Ensino, Rio de Janeiro, RJ 22281-100, Brazil*

[4]*Department of Physics, National Taiwan Normal University, Taipei 106, Taiwan*

[5]*Institute of Physics, Ecole Polytechnique Fédérale de Lausanne (EPFL), CH-1015 Lausanne, Switzerland*

[6]*Instituto de Física, UFRJ, Caixa Postal 68528, Rio de Janeiro, RJ 21941-972, Brazil*

(Received 27 May 2023; accepted 18 October 2023; published 20 November 2023)

Time-correlated Stokes–anti-Stokes (SaS) scattering has been studied in different transparent media, more frequently in diamond. While the nonclassical nature of the SaS scattered photons has been well established, the presence of entanglement in this spontaneous four-wave mixing process has not been demonstrated. Here, we show the violation of the Bell-type Clauser-Horne-Shimony-Holt inequality for the polarization of SaS photon pairs near a Raman resonance in diamond. The degree of entanglement depends on the detuning of the photon pairs from the degenerate two-photon pump and on the orientation of the polarization of the incident light with respect to the crystallographic orientation of the sample. This result opens up the possibility to tailor the quantum state of photon pairs without stringent constraints of phase matching and to combine quantum optics and SaS Raman spectroscopy for new applications in materials science and quantum information.

DOI: 10.1103/PhysRevA.108.L051501

Raman scattering is the inelastic scattering of light by matter, where incident photons lose (Stokes) or gain (anti-Stokes) energy from a material. Most commonly the energy exchanged between the photon and the medium is a phonon. Of particular interest is the phenomenon where the same phonon generated in the Stokes process is absorbed in an anti-Stokes process, generating a pair of quantum correlated Stokes–anti-Stokes (SaS) photons [1–4]. This process is a special type of degenerate four-wave mixing, where two incident photons of the same energy $\hbar\omega_L$ are annihilated inside the material medium to create two photons of different energies $\hbar\omega_S$ and $\hbar\omega_{aS}$, fulfilling energy conservation, $2\hbar\omega_L = \hbar\omega_S + \hbar\omega_{aS}$ (see Fig. 1) [5]. The four-wave mixing process can have a purely electronic microscopic origin [Fig. 1(a)], or it can be mediated by a phonon [Fig. 1(b)]. The phonon-mediated process is clearly distinguishable when resonance is obtained [Fig. 1(b)(ii)], i.e., when $\omega_{S,aS} = \omega_L \pm \omega_{\rm ph}$, where the $\pm$ stands for the anti-Stokes/Stokes scattering and $\hbar\omega_{\rm ph}$ is the phonon energy [6,7]. When tuned out of resonance [Figs. 1(b)(i) and 1(b)(iii)], the phononic SaS pairing can still be mediated by a virtual phonon, having, in this case, an intriguing parallel with the BCS theory for superconductivity [8–11].

In condensed matter physics, the uncorrelated Stokes to anti-Stokes intensity ratio gives the local temperature [2]. Under short pulse excitation, however, the Stokes–anti-Stokes correlation generates rich phenomena in the light-matter interaction [12–17], including their uses to create quantum information transmission protocols [18,19], and to study one-phonon Fock states [20]. This phenomenon is broadly observed, including in liquids [8,21,22], H gas [23], and in nonvibrational related Raman scattering [24,25], among others. Diamond is, however, the preferred material to study such phenomena [9,20,26–29], where the dependence on excitation laser power [9,27], Raman shift and momenta [9], and lifetimes for both resonant (real phonon) and nonresonant (virtual phonon) processes [29] have been explored.

While the nonclassical correlations between SaS photons in diamond are well established, entanglement has been demonstrated only when two interfering pathways are engineered, such as two different samples [30], or a time bin with two different pulses [31]. What is missing is a report on the presence of entanglement in the fundamental four-wave mixing process in diamond. Here, we demonstrate polarization entanglement in SaS photon pairs generated through the superposition of distinct microscopic pathways. In our experiment, the electronic and vibrational four-wave mixing processes shown in Figs. 1(a) and 1(b) collaborate to produce pairs of photons entangled in polarization, verified using the Bell-type Clauser-Horne-Shimony-Holt (CHSH) inequality. The presence of entanglement depends on the crystallographic orientation of the sample with respect to the pump polarization and on the spectral detuning of the photon pairs from the vibrational resonance, which controls the respective contributions of the two pathways illustrated in Figs. 1(a) and 1(b).

Figure 2 illustrates the experimental system, which combines a Raman spectrometer with the time-correlated single-photon counting (TCSPC) apparatus. A 200-fs pulsed MIRA 900F laser tuned at 785 nm with a 76 MHz repetition rate was powered by a Verdi G10 laser from Coherent. The laser with polarization horizontal (H) with respect to the laboratory reference frame departing from the MIRA 900F passes through a half-wave plate (HWP) and a polarized beam splitter (PBS) to control power and convert polarization

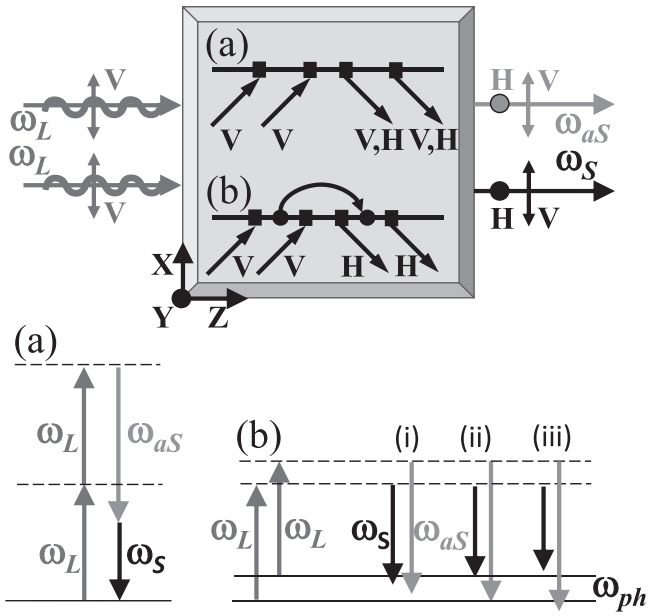

FIG. 1. Microscopic model evidencing the paths where two photons from a laser (ω_L) generate an SaS pair (ω_S and ω_{aS}): (a) purely electronic four-wave mixing; (b) phonon-mediated process, which can be resonant (ii) or detuned out of resonance: (i) negative detuning; (iii) positive detuning. V, H are the orthogonal light polarizations. X, Y, Z are the diamond crystallographic axes.

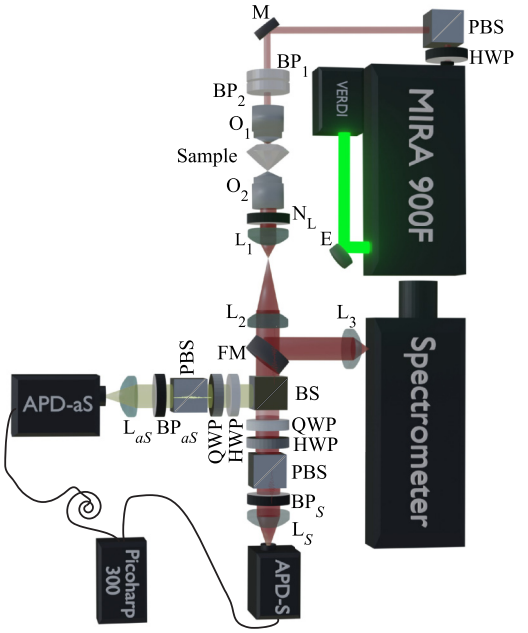

FIG. 2. Schematics of the experimental setup. (E) dielectric mirror for high power, (HWP) half-wave plate, (PBS) polarized beam splitter, (M) silver mirror, ($BP_{1,2}$) interference bandpass filter, (O_1) objective for focusing the excitation laser [20×, numerical aperture (NA) 0.5], (O_2) objective for collecting the scattered signal (100×, NA 0.9), (N_L) notch filter, ($L_{1,2,3,S,aS}$) planoconvex achromatic lenses, (FM) flip mirror, (BS) 50/50 beam splitter, (QWP) quarter-wave plate, ($BP_{S,aS}$) bandpass interference filter to Stokes, anti-Stokes.

to vertical (V) before reaching the sample. With the flip mirror (FM in Fig. 2) in place, the sample can be spectrally characterized through conventional Raman spectroscopy [see Fig. 3(a)]. When the FM is removed, the scattered light is sent to a 50/50 beam splitter (BS), following to a half-wave plate (HWP), a quarter-wave plate (QWP), and a polarized beam splitter (PBS), which are used to select the polarizations of the S and aS photons. After the PBS, bandpass interference filters centered on ω_{aS} and on ω_S ($BP_{aS,S}$) are used for selecting the desired signals. Different $BP_{S,aS}$ are utilized to probe the different spectral regions. The filtered signals are focused on avalanche photodiode detectors (APDs, Excelitas model SPCM-AQRH-14) using lenses L_S and L_{aS}.

The sample is a highly pure diamond grown by the chemical vapor deposition (CVD) process [type IIac Diacell design, (100) oriented], with the laser propagating along the [001] direction of the crystal. The sample is mounted on a rotation stage so that the angle θ between the diamond crystallographic axes and the incident laser polarization can be varied. $\theta = 0°$ stands for the sample [100] direction along V and $\theta = 90°$ stands for the sample [100] direction along H.

Figures 3(b)–3(f) present the results of energy- and polarization-resolved time-correlated SaS photon pair detection rates (I_{SaS}) for three spectral regions: detuned from resonance with $|\omega_L - \omega_{S,aS}| < \omega_{\rm ph}$ [Figs. 3(b) and 3(e)]; in resonance with the phonon, $|\omega_L - \omega_{S,aS}| = \omega_{\rm ph}$ [Figs. 3(c) and 3(f)]; and detuned from resonance with $|\omega_L - \omega_{S,aS}| > \omega_{\rm ph}$ [Figs. 3(d) and 3(g)]. The top row [Figs. 3(b)–3(d)] stands for $\theta = 0°$ and the bottom row [Figs. 3(e)–3(g)] for $\theta = 45°$, where for $\theta = 0°$, $V = X$ in Fig. 1, while for $\theta = 45°$, $V = X + Y$, which are the two inequivalent high-symmetry directions in the XY plane of the cubic diamond crystal. Light is propagating along Z. The observed normalized second-order degree of correlation $g^2(\tau = 0)$ always exceeds the classical limit 2 [28], indicating quantum correlated intensities.

As shown in Figs. 3(b)–3(f) the SaS photon pair is always observed with the same polarization, i.e., either in $V_S V_{aS}$ or $H_S H_{aS}$, with practically no signal being observed in $V_S H_{aS}$ or $H_S V_{aS}$. For $\theta = 0°$ (top row), both $V_S V_{aS}$ and $H_S H_{aS}$ are seen, while for $\theta = 45°$ (bottom row) only the $V_S V_{aS}$ signal can be seen. Notice from Fig. 3 that the amount of $H_S H_{aS}$ signal varies much more than the amount of $V_S V_{aS}$ signal when changing the spectral region, $H_S H_{aS}$ being significantly larger in resonance. Comparing the counts in the top and bottom rows, it appears that the $H_S H_{aS}$ signal observed when $\theta = 0°$ is converted to $V_S V_{aS}$ when $\theta = 45°$.

Out of the measurements displayed in Fig. 3, there are, in principle, two Raman shifts at which entangled polarization states could be produced when the polarization of the incident laser is oriented along the diamond crystallographic axis $\theta = 0°$: ±900 and ±1332 $\rm cm^{-1}$. In both cases, the statistics show a clear polarization correlation in the $|V_S, V_{aS}\rangle$, $|H_S, H_{aS}\rangle$ basis. Here, as is customary when discussing photon pairs produced by parametric down-conversion, we neglect the part of the biphoton wave function with more than one photon pair and use the shorthand notation $|V_S, V_{aS}\rangle$ ($|H_S, H_{aS}\rangle$) to designate a pair of vertically (horizontally) polarized SaS photons created out the vacuum. While we have not measured the Schmidt number of the biphoton wave function, it is likely that several pairs of temporal modes are populated in the process,

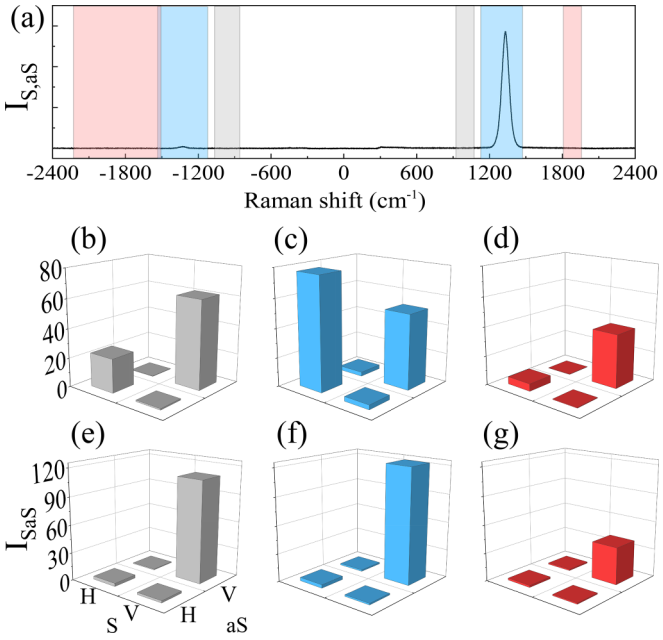

FIG. 3. (a) Unpolarized spontaneous Raman spectrum from the diamond crystal under pulsed excitation at 785 nm. Stokes (anti-Stokes) photons are at positive (negative) Raman shifts. (b)–(g) Time-correlated SaS photon pair intensity (I_{SaS}) for the three sets of spectral filters colored in (a): (b), (e) $|\omega_L - \omega_{S,aS}| = 900$ cm^{-1} (gray region); (c), (f) $|\omega_L - \omega_{S,aS}| = 1332$ cm^{-1} (blue region); (d), (g) $|\omega_L - \omega_{S,aS}| = 1900$ cm^{-1} (red region). (b)–(d) $\theta = 0°$, (e)–(g) $\theta = 45°$. For each spectral region, a set of bandpass filters was utilized: (b), (e) Stokes filter: 850/10; anti-Stokes filter: 730/10. (c), (f) Stokes: 875/25; anti-Stokes: 711/25. (d), (g) Stokes: 920/10; anti-Stokes: 685/40. A/B refer to the filters' center wavelength (A) and bandwidth (B) in nm; they define the gray, blue, and red spectral regions indicated in (a) where measurements in (b)–(g) took place. I_{SaS} were corrected to account for the spectral efficiency of the experimental apparatus and different excitation powers, given in counts/cm^{-1} mW^2 s.

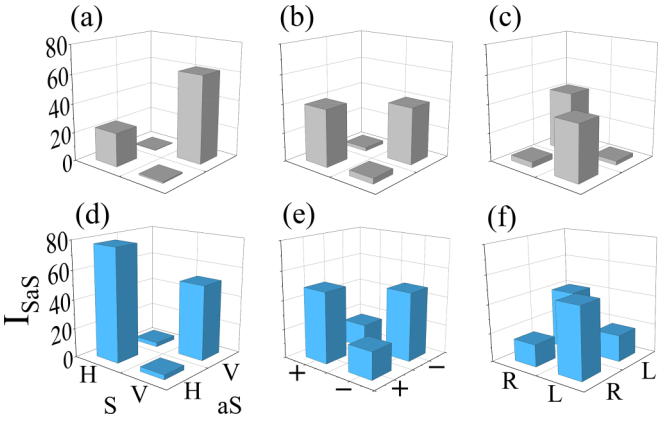

FIG. 4. I_{SaS} for a Raman shift of (a)–(c) ± 900 cm^{-1} and (d)–(f) ± 1332 cm^{-1}, both at $\theta = 0°$. The incident light is always polarized in V, and the Stokes and anti-Stokes scattered light are polarized at three different basis: (a), (d) VH [same as Figs. 3(b) and 3(c), respectively], (b), (e) $+-$, and (c), (f) RL.

but the CHSH parameter discussed below is not affected by the number of collected modes, as long as all pairs feature entanglement.

In order to investigate whether the generated state is classically mixed or entangled, we focused first on the 900 cm^{-1} pairs [Fig. 3(a)] and took a two-step approach: First, we rotated the polarization analyzers to also observe the pairs in the linearly polarized $+-$ and in the circularly polarized RL bases. The results, shown in Figs. 4(a)–4(c), still display correlated pairs of polarization in both bases, ruling out a statistical mixture, for which all the populations should be equal, and pointing to an entangled state of the type

$$|\psi\rangle_{S,aS} = c_1|V_S, V_{aS}\rangle + c_2|H_S, H_{aS}\rangle. \quad (1)$$

Here, $c_1 = \sqrt{0.72}$ and $c_2 = \sqrt{0.28}$ can be extracted from the relative counts of $V_S V_{aS}$ and $H_S H_{aS}$ pairs displayed in Fig. 3(a) and the phase $(+)$ is consistent with the presence of $\{++, --, RL, LR\}$ pairs (an opposite phase would generate $\{+-, -+, RR, LL\}$ correlations). This state is very close to the $|\phi^+\rangle$ Bell state, $|\psi\rangle_{S,aS} = \sqrt{0.95}|\phi^+\rangle + \sqrt{0.05}|\phi^-\rangle$, where $|\phi^\pm\rangle = (|VV\rangle \pm |HH\rangle)/\sqrt{2}$. Second, we validated this entangled state by performing a standard Bell-type CHSH inequality, with the angles of the polarization analyzers properly chosen for the inequality to be maximally violated by the $|\phi^+\rangle$ state (see details in the Supplemental Material [32]). We obtained $|S| = 2.61 \pm 0.03$ for the CHSH violation, which is much larger than the classically correlated limit of $|S| = 2$ and close to the predicted value of $|S| = 2.68$ for the chosen angles and the state in Eq. (1). The error in S was estimated with a Monte Carlo simulation. The difference between the value predicted by the theory and the one obtained experimentally for $|S|$ can be explained by a combination of the effects of a small phase in c_2 ($\phi \leqslant 0.1\pi$) and a small degree of state mixing (purity higher than 0.95), both values obtained from the data described in the Supplemental Material [32]. Therefore, the SaS state is indeed very close to $|\phi^+\rangle$.

For a Raman shift resonant with the optical phonon, on the other hand, the violation is marginal, with $|S| = 2.05 \pm 0.16$, a possible consequence of the much larger background of uncorrelated photons due to the large single-photon Stokes scattering rate. This result is consistent with Figs. 4(d)–4(f), which shows a smaller degree of correlation in the distribution of SaS pairs in the $+-$ and RL polarization basis. The downgrade of the correlation at the Raman resonance may result from a statistical mixture of the SaS entangled pairs with unentangled three-photon states. Three-photon states are mainly due to the sum of a standard single-photon Stokes scattering and a SaS pair. The detectors do not distinguish between two- and three-photon events and the measurement apparatus ends up bunching them in the same correlation statistics. This behavior was already analyzed in previous papers as the physical origin of the severe lowering of the value of the zero-delay cross-correlation function $g^2_{SaS}(0)$ at the Raman resonance [11,27]. We have confirmed it by performing the tomography of the postselected two-photon states, obtaining a purity ($\mathrm{Tr}[\rho^2]$) of around 0.6 (see the Supplemental Material [32]), which indicates a largely mixed polarization state. For the $\theta = 45°$ orientation we seek no CHSH violation because essentially all the photons are generated at the same polarization. The same can be said for the 1900 cm^{-1} pairs

because the H_S, H_{aS} counts are too low and the time-correlated pairs are of the same order of the accidental counts [9,11]. At this spectral range the overall polarization state is always essentially $|V_S, V_{aS}\rangle$, regardless of the crystallographic orientation.

The observed polarization entanglement of photon pairs at ± 900 cm^{-1} Raman shift is proposed to result from the coexistence of two independent pathways contributing to spontaneous four-wave mixing [6,7]: The $\chi^{(3)}$ tensor is the sum of one nonresonant contribution $\chi^{(3)}_{\rm NR}$ from electronic transitions that are far-detuned from any energy involved in the four-wave mixing process, plus one (near) resonant term $\chi^{(3)}_R$ that results from vibrational Raman scattering. Using the convention of Ref. [7], where the stimulated counterpart of the process studied here was investigated, we label the indices of the $\chi^{(3)}$ tensor in the following order, $\chi^{(3)}_{ijkl}(\omega_{aS}, \omega_L, \omega_L, \omega_S)$, where $i, j, k, l = X, Y = V, H$, the latter equality being valid for $\theta = 0^\circ$. For example, the tensor element $\chi^{(3)}_{HVVH}$ is responsible for the creation of H_S, H_{aS} pairs under V polarized pumping.

Now, since diamond is a cubic system (O_h point symmetry group), the nonresonant (purely electronic) part of the tensor contains only three distinct nonzero contributions: $\chi^{(3)}_{\rm NR} = \chi^e_{iiii} + \chi^e_{ijji} + \chi^e_{iijj}$. Together with the experimental pump geometry for $\theta = 0^\circ$, it means that only χ^e_{VVVV} and χ^e_{HVVH} contribute, leading to V_S, V_{aS} and H_S, H_{aS} photon pairs, respectively. Further, it was shown in Ref. [7] that $|\chi^e_{VVVV}| \simeq 3|\chi^e_{HVVH}|$, so that we would expect nine times more V_S, V_{aS} pairs than H_S, H_{aS} pairs if only the electronic contribution were at play. The form of the resonant (Raman) contribution is further constrained by the symmetry of the optical phonon that belongs to the triply degenerate T_{2g} irreducible representation, so that $\chi^{(3)}_R = \chi^R_{HVVH}$ in the experimental geometry for $\theta = 0^\circ$. Note also that the phase of $\chi^{(3)}_R$ experiences a change of π when the Raman shift crosses the vibrational resonance so that photons generated from this pathway at larger Raman shifts interfere destructively with the ones resulting from χ^e_{HVVH} [7].

Altogether, if we neglect χ^e_{HVVH} for the simplicity of the discussion, we find that for a V polarized pump and $\theta = 0^\circ$ the form of the third-order nonlinear susceptibility tensor is just $\chi^e_{VVVV} + \chi^R_{HVVH}$, where the magnitude of the first term is detuning independent while the magnitude of the second term strongly depends on the detuning of the detected photon pairs with respected to the vibrational Raman shift. For a suitable choice of detuning (e.g., around ± 900 cm^{-1} as we found here) the electronic and vibrational contributions have similar magnitudes. Moreover, since photon pairs produced by the two pathways are otherwise indistinguishable in their temporal and spatial modes, except for their polarizations, we do predict that the biphoton state should be of the form $|\psi\rangle_{SaS} = c_1|V_S, V_{aS}\rangle + c_2|H_S, H_{aS}\rangle$. Future work is needed to explore to what extent the coefficients c_1 and c_2 can be adjusted by spectral filtering, allowing for a tailored quantum state.

To conclude, we have demonstrated the production of polarization-entangled photon pairs in a diamond sample through a four-wave mixing process. The entanglement is obtained only when the crystal orientation favors two distinct paths for generating the four-wave mixing. For light reaching the sample in the [100] direction, entanglement is obtained when the incident laser is polarized along one of the crystallographic axes, since electronic four-wave mixing can either conserve or change, but it preferably conserves the polarization of both Stokes and anti-Stokes photons, while vibronic four-wave mixing (SaS scattering) necessarily changes their polarizations. Entanglement comes from the indistinguishability of both processes, i.e., because it is not possible, even in principle, to determine which process took place. As a result, the superposition of the two possible pathways generates pairs of photons in the entangled polarization state $|\psi\rangle_{SaS} = c_1|V_S, V_{aS}\rangle + c_2|H_S, H_{aS}\rangle$. Interestingly, our results indicate that the different electronic and phononic pathways can interfere in order to engineer the polarization of the two-photon quantum state when light travels in the crystal in well-defined geometries: Which process (electronic and phononic) took place is therefore no longer a valid question. These results display entanglement generated by "which physical process" indeterminacy and they open up the possibility to explore Raman spectroscopy in different ways. Since the SaS scattering has been observed in many different transparent media, this type of entanglement may be more general, conditioned to the presence of different indistinguishable four-wave mixing microscopic paths within the medium.

The authors acknowledge financial support by Fapemig (TEC-RED-00282-16, APQ-01860-22), CNPq (302775/2018-8, 442521/2019-7, 313158/2022-3), FAPERJ (E-26/202.576/2019, E-26/200.307/2023), CAPES-PRINT/UFMG, and JSPS Kakenhi (No. JP22H00283) and Yushan Fellow Program.

[1] D. N. Klyshko, Correlation between the Stokes and anti-Stokes components in inelastic scattering of light, Sov. J. Quantum Electron. **7**, 755 (1977).

[2] C. A. Parra-Murillo, M. F. Santos, C. H. Monken, and A. Jorio, Stokes–anti-Stokes correlation in the inelastic scattering of light by matter and generalization of the Bose-Einstein population function, Phys. Rev. B **93**, 125141 (2016).

[3] A. V. A. Guimarães, M. F. Santos, A. Jorio, and C. H. Monken, Stokes–anti-Stokes light-scattering process: A photon-wave-function approach, Phys. Rev. A **102**, 033719 (2020).

[4] K. Thapliyal and J. Peřina, Jr., Ideal pairing of the Stokes and anti-Stokes photons in the Raman process, Phys. Rev. A **103**, 033708 (2021).

[5] N. Bloembergen, *Nonlinear Optics* (W. A. Benjamin, New York, 1974).

[6] M. D. Levenson, C. Flytzanis, and N. Bloembergen, Interference of resonant and nonresonant three-wave mixing in diamond, Phys. Rev. B **6**, 3962 (1972).

[7] M. D. Levenson and N. Bloembergen, Dispersion of the nonlinear optical susceptibility tensor in centrosymmetric media, Phys. Rev. B **10**, 4447 (1974).

[8] A. Saraiva, F. S. de Aguiar Júnior, R. de Melo e Souza, A. P. Pena, C. H. Monken, M. F. Santos, B. Koiller, and A. Jorio, Photonic counterparts of Cooper pairs, Phys. Rev. Lett. **119**, 193603 (2017).

[9] F. S. de Aguiar Júnior, A. Saraiva, M. F. Santos, B. Koiller, R. M. Souza, A. P. Pena, R. A. Silva, C. H. Monken, and A. Jorio, Stokes–anti-Stokes correlated photon properties akin to photonic Cooper pairs, Phys. Rev. B **99**, 100503(R) (2019).

[10] Y. Zhang, L. Zhang, and Y.-Y. Zhu, Generation of photonic Cooper pairs in nanoscale optomechanical waveguides, Phys. Rev. A **98**, 013824 (2018).

[11] F. S. de Aguiar Júnior, C. H. Monken, M. F. Santos, R. de Melo e Souza, A. Saraiva, B. Koiller, and A. Jorio, Physical properties of photonic Cooper pairs generated via correlated Stokes–anti-Stokes Raman scattering, Physica Status Solidi B **256**, 1900218 (2019).

[12] K. Kneipp, Y. Wang, H. Kneipp, I. Itzkan, R. R. Dasari, and M. S. Feld, Population pumping of excited vibrational states by spontaneous surface-enhanced Raman scattering, Phys. Rev. Lett. **76**, 2444 (1996).

[13] A. G. Brolo, A. C. Sanderson, and A. P. Smith, Ratio of the surface-enhanced anti-Stokes scattering to the surface-enhanced Stokes-Raman scattering for molecules adsorbed on a silver electrode, Phys. Rev. B **69**, 045424 (2004).

[14] E. Le Ru and P. Etchegoin, Vibrational pumping and heating under SERS conditions: Fact or myth? Faraday Discuss. **132**, 63 (2006).

[15] P. Roelli, C. Galland, N. Piro, and T. J. Kippenberg, Molecular cavity optomechanics as a theory of plasmon-enhanced Raman scattering, Nat. Nanotechnol. **11**, 164 (2016).

[16] M. K. Schmidt, R. Esteban, A. González-Tudela, G. Giedke, and J. Aizpurua, Quantum mechanical description of Raman scattering from molecules in plasmonic cavities, ACS Nano **10**, 6291 (2016).

[17] Y. Zhang, J. Aizpurua, and R. Esteban, Optomechanical collective effects in surface-enhanced Raman scattering from many molecules, ACS Photonics **7**, 1676 (2020).

[18] A. Kuzmich, W. P. Bowen, A. D. Boozer, A. Boca, C. W. Chou, L. M. Duan, and H. J. Kimble, Generation of nonclassical photon pairs for scalable quantum communication with atomic ensembles, Nature (London) **423**, 731 (2003).

[19] D. G. England, P. J. Bustard, J. Nunn, R. Lausten, and B. J. Sussman, From photons to phonons and back: A THz optical memory in diamond, Phys. Rev. Lett. **111**, 243601 (2013).

[20] S. T. Velez, K. Seibold, N. Kipfer, M. D. Anderson, V. Sudhir, and C. Galland, Preparation and decay of a single quantum of vibration at ambient conditions, Phys. Rev. X **9**, 041007 (2019).

[21] V. Vento, S. Tarrago Velez, A. Pogrebna, and C. Galland, Measurement-induced collective vibrational quantum coherence under spontaneous Raman scattering in a liquid, Nat. Commun. **14**, 2818 (2023).

[22] M. Kasperczyk, F. S. de Aguiar Júnior, C. Rabelo, A. Saraiva, M. F. Santos, L. Novotny, and A. Jorio, Temporal quantum correlations in inelastic light scattering from water, Phys. Rev. Lett. **117**, 243603 (2016).

[23] P. J. Bustard, J. Erskine, D. G. England, J. Nunn, P. Hockett, R. Lausten, M. Spanner, and B. J. Sussman, Nonclassical correlations between terahertz-bandwidth photons mediated by rotational quanta in hydrogen molecules, Opt. Lett. **40**, 922 (2015).

[24] M. Bashkansky, F. K. Fatemi, and I. Vurgaftman, Quantum memory in warm rubidium vapor with buffer gas, Opt. Lett. **37**, 142 (2012).

[25] K. F. Reim, J. Nunn, V. O. Lorenz, B. J. Sussman, K. C. Lee, N. K. Langford, D. Jaksch, and I. A. Walmsley, Towards high-speed optical quantum memories, Nat. Photonics **4**, 218 (2010).

[26] K. C. Lee, B. J. Sussman, M. R. Sprague, P. Michelberger, K. F. Reim, J. Nunn, N. K. Langford, P. J. Bustard, D. Jaksch, and I. A. Walmsley, Macroscopic non-classical states and terahertz quantum processing in room-temperature diamond, Nat. Photonics **6**, 41 (2012).

[27] M. Kasperczyk, A. Jorio, E. Neu, P. Maletinsky, and L. Novotny, Stokes–anti-Stokes correlations in diamond, Opt. Lett. **40**, 2393 (2015).

[28] M. D. Anderson, S. Tarrago Velez, K. Seibold, H. Flayac, V. Savona, N. Sangouard, and C. Galland, Two-color pump-probe measurement of photonic quantum correlations mediated by a single phonon, Phys. Rev. Lett. **120**, 233601 (2018).

[29] F. S. de Aguiar Júnior, M. F. Santos, C. H. Monken, and A. Jorio, Lifetime and polarization for real and virtual correlated Stokes–anti-Stokes Raman scattering in diamond, Phys. Rev. Res. **2**, 013084 (2020).

[30] K. C. Lee, M. R. Sprague, B. J. Sussman, J. Nunn, N. K. Langford, X. M. Jin, T. Champion, P. Michelberger, K. F. Reim, D. England, D. Jaksch, and I. A. Walmsley, Entangling macroscopic diamonds at room temperature, Science **334**, 1253 (2011).

[31] S. T. Velez, V. Sudhir, N. Sangouard, and C. Galland, Bell correlations between light and vibration at ambient conditions, Sci. Adv. **6**, eabb0260 (2020).

[32] See Supplemental Material at http://link.aps.org/supplemental/10.1103/PhysRevA.108.L051501 for more details on the CHSH parameter analysis and the results of state tomography for the selected states that violates the CHSH inequality.